Physica D 318–319 (2016) 84–90

Contents lists available at ScienceDirect

Physica D

journal homepage: www.elsevier.com/locate/physd

Reaction–diffusion–advection approach to spatially localized treadmilling aggregates of molecular motors

Arik Yochelis [a,*], Tomer Bar-On [b], Nir S. Gov [b,*]

[a] Department of Solar Energy and Environmental Physics, Swiss Institute for Dryland Environmental and Energy Research, Blaustein Institutes for Desert Research (BIDR), Ben-Gurion University of the Negev, Sede Boqer Campus, Midreshet Ben-Gurion 84990, Israel

[b] Department of Chemical Physics, The Weizmann Institute of Science, Rehovot 76100, Israel

HIGHLIGHTS

- Reaction–diffusion–advection model for the formation of spatially localized molecular-motor aggregates (pulses).
- Analytic trends of pulses properties via model parameters: shape and propagation velocity.

ARTICLE INFO

Article history:
Received 19 July 2015
Received in revised form
27 October 2015
Accepted 28 October 2015
Available online 12 January 2016

Keywords:
Molecular-motors
Pattern formation
Pulses

ABSTRACT

Unconventional myosins belong to a class of molecular motors that walk processively inside cellular protrusions towards the tips, on top of actin filament. Surprisingly, in addition, they also form retrograde moving self-organized aggregates. The qualitative properties of these aggregates are recapitulated by a mass conserving reaction–diffusion–advection model and admit two distinct families of modes: *traveling waves* and *pulse trains*. Unlike the traveling waves that are generated by a linear instability, pulses are nonlinear structures that propagate on top of linearly stable uniform backgrounds. Asymptotic analysis of isolated pulses via a simplified reaction–diffusion–advection variant on large periodic domains, allows to draw qualitative trends for pulse properties, such as the amplitude, width, and propagation speed. The results agree well with numerical integrations and are related to available empirical observations.

1. Introduction

Molecular motors facilitate a mean of transport within cells, and are especially vital to chemical exchange in actin-based cellular protrusions [1], such as filopodia [2] and stereocilia [3]. Unconventional myosins (UM), constitute arguably the most important family of processive motors, moving and transporting chemical cargos to and from the plus-ends (growing tips) of actin-filaments; except for myosin-VI which is a minus-end directed motor. Thus, dynamical properties of UM are central to cell functionalities, example of which include migration, morphology, communication and morphogenesis [4,5].

Despite the tendency of UM to accumulate at the protrusion tips, where the plus ends of the actin filaments are located, there are many observations of retrograde motion of aggregates towards the protrusion base. These self-organized aggregates are common to both filopodia and stereocilia and are associated with myosin-X [6–9], myosin-XV [10], myosin-III [11] and myosin-Va [8]. The qualitative mechanisms of these motor aggregates can be captured through a continuum reaction–diffusion–advection model that constitutes three basic types of motors [12]: freely diffusing, actin-bound stalled motors advected by the retrograde flow of actin towards the protrusion base, and actin-bound processive motors that walk towards the tip. In particular, the model allows to distinguish between two transport modes: traveling waves and pulse trains.

Here we aim to develop a better understanding of *isolated* pulses, by further simplification of the original model through which only two motor types are considered: processive and stalled. Using asymptotic analysis in a co-moving coordinate frame, we derive trends for the amplitude, velocity and width of the pulses. We show that these analytically derived forms agree well with direct numerical integrations and also with pulses obtained in the original model, i.e., a model that includes also freely diffusing motors [12]. Finally, we confront the obtained results with experi-

* Corresponding authors.
E-mail addresses: yochelis@bgu.ac.il (A. Yochelis), nir.gov@weizmann.ac.il (N.S. Gov).

http://dx.doi.org/10.1016/j.physd.2015.10.023
0167-2789/

mentally observed features and make suggestions for future experiments.

2. Reaction–diffusion–advection framework for self-organization of molecular motors

Self-organization of molecular motors inside a cellular protrusion can be described by an effective one-dimensional projection of the emergent dynamics since the protrusions are usually thin compared to their length. The equations of motion then qualitatively incorporate continuum transport and interactions between three forms of the molecular motors [12]:

- m_f, motors which are not physically connected to actin filaments and thus freely diffuse with diffusion coefficient D. If the diffusion is very fast $D \gg v_b h$ (where v_b is the retrograde speed of the actin and h is the length of the protrusion), or in an unbounded volume, it acts to diminish and eventually abolish the pulses [12].
- m_b, stalled motors that are physically anchored to the actin filaments and are transported towards the cell (protrusion base) with roughly the treadmilling velocity of the actin filaments v_b. However even if stalled, these motors can still exhibit random forward and backward steps [8] which result in a small effective diffusion (D_b) along the actin filaments [13], i.e. $D_b/D \ll 1$. Such stalled movements of motors could arise when motors lose their cargo, or enter a self-inhibiting conformation [14,15].
- m_w, processive motors that are only walking against the actin polymerization towards the protrusion tip with velocity $v_w - v_b$ ($|v_b/v_w| \gg 1$).

The equations of motion read as [12]:

$$\frac{\partial m_f}{\partial t} = -\frac{\partial J_f}{\partial z} + \underbrace{\mathcal{L}_f\left(m_f, m_b, m_w\right)}_{\text{linear reaction}}, \tag{1a}$$

$$\frac{\partial m_b}{\partial t} = -\frac{\partial J_b}{\partial z} + \underbrace{\mathcal{L}_b\left(m_f, m_b, m_w\right)}_{\text{linear reaction}} + \underbrace{\mathcal{N}\left(m_b, m_w\right)}_{\text{nonlinear reaction}}, \tag{1b}$$

$$\frac{\partial m_w}{\partial t} = -\frac{\partial J_w}{\partial z} + \underbrace{\mathcal{L}_w\left(m_f, m_b, m_w\right)}_{\text{linear reaction}} - \underbrace{\mathcal{N}\left(m_b, m_w\right)}_{\text{nonlinear reaction}}, \tag{1c}$$

where the respective linear operators correspond to on/off transition rates between the free, stalled, processive motors and due to mass conservation of the motors $\mathcal{L}_f + \mathcal{L}_b + \mathcal{L}_w = 0$. The nonlinear reactions are related only to motors that propagate along the actin filaments since only these motors can create aggregates bearing a similarity to formation of traffic jams [15]. The local reaction terms in the three-state motor model and the fluxes in (1) are respectively, given by:

$$\mathcal{L}_f = -\left(k_1^n + k_2^n\right) m_f + k_1^f m_b + k_2^f m_w, \tag{2}$$

$$\mathcal{L}_b = k_1^n m_f - \left(k_1^f + k_3^n\right) m_b, \tag{3}$$

$$\mathcal{L}_w = k_2^n m_f - k_2^f m_w + k_3^n m_b, \tag{4}$$

$$\mathcal{N} = k_3^f \left(1 + k_{bw} m_b^2\right) m_w, \tag{5}$$

and

$$J_f = -D\frac{\partial m_f}{\partial z}, \tag{6a}$$

$$J_b = -D_b\frac{\partial m_b}{\partial z} - m_b v_b, \tag{6b}$$

$$J_w = m_w(v_w - v_b) \tag{6c}$$

where k_{bw} is a nonlinear transition rate and $k_1^{n,f}$, $k_2^{n,f}$, $k_3^{n,f}$ are first order on/off transition rates, respectively. Briefly, the model (1) describes an effective one-dimensional projection of the emergent dynamics along the actin bundle comprising the core of the cellular protrusion. Since the protrusions are usually thin compared to their length, we ignore variations within the cross-section of the protrusion. Furthermore, for simplicity we ignore dynamical variations in the length h of the protrusion. This is reasonable since many filopodia are observed to be stable on a time-scale that is long compared to the frequency of formation of retrograde motor aggregates [12], as filopodia are often stabilized by adhesion to the external substrate. In addition, we treat the retrograde flow of the actin filaments v_b as constant. This flow is driven by the actin polymerization at the protrusion tip, and by the pull of myosin-II motors inside the cell cytoplasm. While the processive motors inside the protrusion could also contribute to this flow, these corrections are neglected in this model.

Eqs. (1) are supplemented with boundary conditions (BCs) that reflect realistic properties of motors [12]:

- At the protrusion base $z = 0$, $\left[m_f, J_b, J_w\right] = \left[m_f^0, -v_b m_b, (v_w - v_b)m_w\right]$, where the concentration of free (and actin-bound) motors is usually very low, i.e., $m_f^0 \to 0$;
- At the protrusion tip $z = h$, since the protrusion is closed there must be an overall zero flux condition which imposes a conversion rate according to $J_b = -\beta J_w, J_f = -(1-\beta)J_w$, where $0 \le \beta \le 1$. Here $\beta = 1$ corresponds to pure transition between the counter propagating subsets $m_w \to m_b$ (processive motors stall at the tip, Fig. 1(b)), while $\beta = 0$ denotes a pure transition to freely diffusing $m_w \to m_f$ (processive motors fall-off the actin bundle at the tip, Fig. 1(a)).

Unlike standard reaction–diffusion systems, mass conservation in the bulk introduces multiplicity of uniform states for which one of the fields, for example m_f can be considered as an additional control parameter. In a companion paper [12], we have demonstrated that pattern selection to traveling waves and pulse trains arise from BCs: for $\beta \to 0$ (Fig. 1(a)), and for small (realistic) values of m_f, the uniform states are linearly stable but the accumulation of motors at the tip arise in pulse trains, while the emergence of traveling waves ($\beta \to 1$) arise through a finite wavenumber instability (Fig. 1(b)), cf. [16]. The pulses are excitable pulses (dissipative solitons) which correspond to homoclinic orbits in the co-moving reference frame [17]. In this paper we focus on their qualitative core properties.

3. Isolated pulses

For isolated pulses, we require linear stability of uniform states by assuming $m_f \to 0$ and $m_f \ll m_b, m_w$, which also keeps fidelity to biology of motors inside the protrusion, i.e., UM usually have a high affinity to the actin filaments, so that the fraction of motors in the freely diffusing state is relatively small [8]. Since the equation of motion for m_f is linear, it is therefore enslaved to the nonlinear behavior of m_b and m_w. Moreover, the minimal requirement for homoclinic orbits in reaction–diffusion systems is a two variable system with differential advection and at least a single diffusing term [17,18], i.e., the role played by the third specie, the freely diffusing state, is negligible from the qualitative point of view. It is therefore, useful to study a simpler version of the model comprising only the processive and stalled species. In what follows, we demonstrate that the simplified model contains not only the ability to sustain propagating pulses, similar to the full

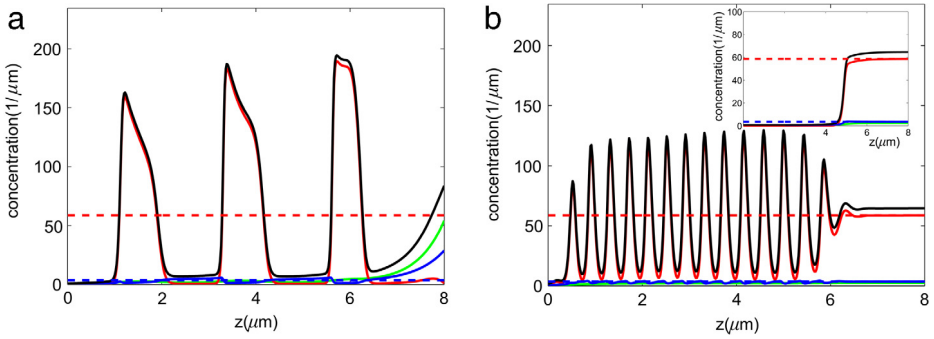

Fig. 1. (a) Numerical solution at a given time showing a typical pulse train profile that emerges at the tip and propagates to the protrusion base [12]; Eqs. (1) were numerically integrated using the boundary condition at the tip of processive motors becoming freely diffusing ($\beta = 0$) and with parameters $m_f^0 = 0.1$, $k_{bw} = 0.05$, $k_3^n = 0.2$, $k_w = 0.02$, $v_b = 0.02$, $v_w = 0.35$, $D_b = 2.5 \cdot 10^{-4}$, $k_1^n = 0.01$, $k_1^f = 0.01$, $k_2^n = 0.3$, $k_2^f = 0.05$. The local concentrations of the stalled, processive and free motors (m_b, m_w, m_f) are denoted by the red, blue and green lines respectively, and the sum of the total concentration is in black. The horizontal dashed red line denotes the concentration of stalled motors in the M^U state. (b) Numerical solution at a given time of TWs that are forming for boundary conditions where at the tip of processive motors are becoming stalled ($\beta = 1$). The inset shows the growth of the M^U state (Eq. (9)) from the tip, before the unstable modes start to grow. Parameters: $m_f^0 = 0.1$, $k_{bw} = 0.05$, $k_3^n = 0.2$, $k_w = 0.02$, $v_b = 0.02$, $v_w = 0.35$, $D_b = 2.5 \cdot 10^{-4}$, $k_1^n = 0.01$, $k_1^f = 0.01$, $k_2^n = 0.3$, $k_2^f = 0.05$. (For interpretation of the references to color in this figure legend, the reader is referred to the web version of this article.)

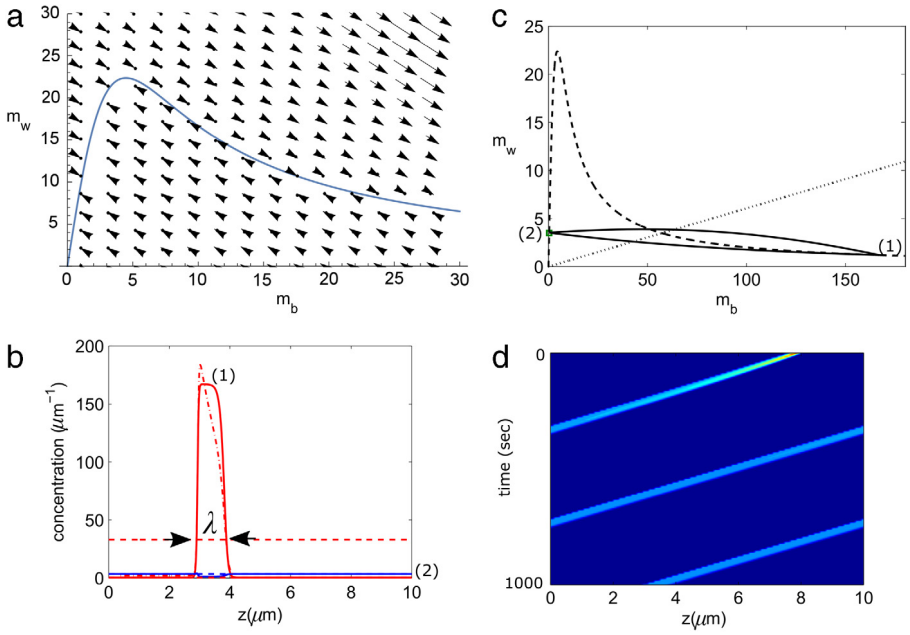

Fig. 2. (a) Locus of uniform solutions (solid line, Eq. (8)) where arrows indicate the flows, along the diagonals that conserve total mass: $m_b + m_w = const$. (b) An isolated pulse profile on a periodic domain, initiated using a Gaussian perturbation in the m_b field. Red (blue) line describes the concentration of stalled m_b (processive m_w) motors, respectively. The bottom horizontal dashed lines (near zero concentrations) indicate the background initial states (m_b, m_w) (using: $m_b = 0.35$) and the top horizontal dashed red line gives the value of m_b at the M^U state (Eqs. (9)). We denote the width of the pulse, λ, at the M^U value while (1) in (b, c) denotes the value of m_b at the peak of the pulse, $m_{b,peak}$. The parameters are the same as in Fig. 1: $D_b = 2.5 \cdot 10^{-4}$, $k_{bw} = 0.05$, $k_b = 0.2$, $k_w = 0.02$, $v_b = 0.02$, $v_w = 0.35$, $m_b^* = 0.35$. For comparison we also plot by the dash–dot red line for a pulse profile obtained through integration of the equivalent 3-species model (1), using $m_f^0 = 0.55$ to ensure that $m_b^* = 0.35$ as in (b). (c) Trajectory (solid line) of the pulse (b) plotted in the (m_b, m_w) plane. The dashed line as in (a) while the dotted line corresponds to the zero-flux condition which by crossing the dashed line marks the M^U state. (d) Space–time plot showing the propagation of a pulse (b); the slope of this line gives the propagation velocity, which is always larger than the treadmilling speed of the actin v_b. The color heat-map gives the local concentration of m_b, with light colors marking larger m_b values. (For interpretation of the references to color in this figure legend, the reader is referred to the web version of this article.)

model (as expected), but also has the advantage of being amenable to analytic analysis.

After exclusion of m_f, the equations for stalled and processive motors read as:

$$\frac{\partial m_b}{\partial t} = D_b \frac{\partial^2 m_b}{\partial z^2} + v_b \frac{\partial m_b}{\partial z} - k_b m_b + k_w \left(1 + k_{bw} m_b^2\right) m_w \tag{7a}$$

$$\frac{\partial m_w}{\partial t} = -(v_w - v_b) \frac{\partial m_w}{\partial z} + k_b m_b - k_w \left(1 + k_{bw} m_b^2\right) m_w \tag{7b}$$

where $k_w \equiv k_3^f$ and $k_b \equiv k_3^n$. This form of the model bears similarity to other autocatalytic models [19].

3.1. Uniform solutions and constrains

Uniform solutions to (7) are given by

$$m_w^* = \frac{k_b}{k_w} \frac{m_b^*}{1 + k_{bw}(m_b^*)^2}. \tag{8}$$

Since our interest is in isolated pulses, we consider periodic domains that are large in comparison to the pulse width. The pulses are being initiated by spatially localized large amplitude perturbations above a stable uniform state (of low motor densities) to which we refer as M^L. This stable uniform state corresponds to solutions of Eq. (8) with low values of m_b, i.e., $m_b < 5$ in Fig. 2(a).

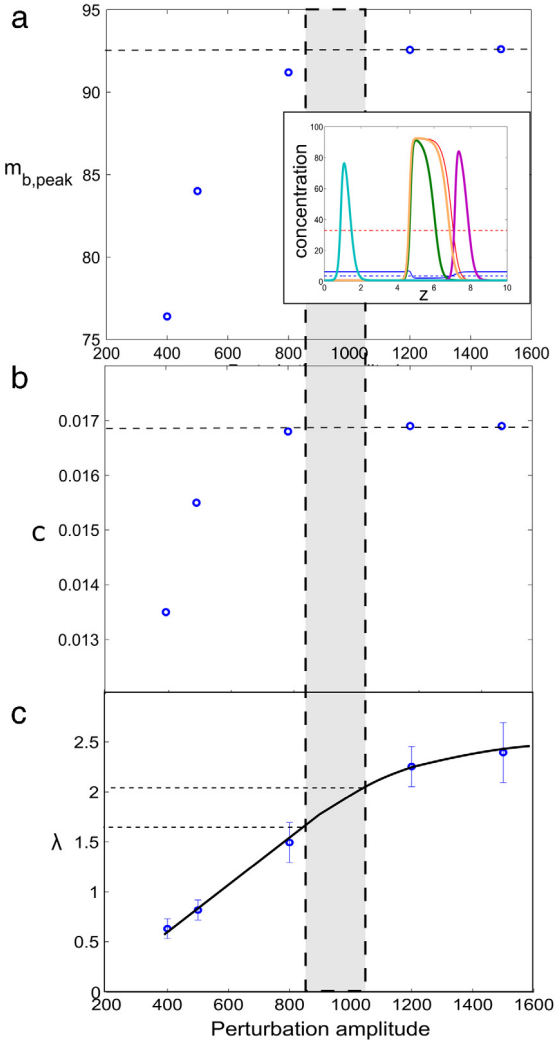

Fig. 3. (a) Pulse amplitude $m_{b,peak}$ and (b) treadmilling velocity c, as a function of the amplitude of the initial Gaussian perturbation applied to m_b field with constant width. The inset in (a), shows several pulses generated by distinct perturbations at $t = 2000$ s. Asymptotically, both $m_{b,peak}$ and c reach saturation, indicated by the horizontal dashed lines. To define the pulse width $\lambda(c)$, we use the smallest amplitude that gives these saturation values (shaded region). Parameters as in Fig. 2.

Fig. 2(b)–(d) shows, a typical profile of a propagating pulse. Such a pulse reaches a steady-state shape, characterized by its amplitude $m_b \equiv m_{b,peak}$ (marked as (1) in Fig. 2(b), (c)), width λ, and constant propagation velocity. It is both expected and verified here that the propagation velocity is always larger than the speed of the actin flow v_b, since it is increased by a finite treadmilling velocity of the motors inside the aggregate.

The upper limiting state M^U satisfies the zero total flux condition, i.e., $m_b^*/m_w^* = v_b/(v_w - v_b)$, for which we obtain (Fig. 2(c)):

$$m_b^u = \sqrt{\frac{k_b(v_w - v_b) - k_w v_b}{k_w k_{bw} v_b}}, \tag{9a}$$

$$m_w^u = \frac{\sqrt{v_b}}{v_w}\sqrt{\frac{k_b(v_w - v_b) - k_w v_b}{k_w k_{bw}}}. \tag{9b}$$

Notably, M^U can be thought of as an attracting slow manifold [20,21], whereby localized initial perturbations with an amplitude much smaller than this state generally decay to the uniform state.

3.2. Analysis of isolated pulses on large domains

For analysis purposes, we define a co-moving coordinate in which, the pulse solutions move in the direction of the actin retrograde flow with a constant speed $v_b + c$, i.e. $m_{b,w}(z,t) = m_{b,w}(\eta)$, where $\eta = z + (v_b + c)t$ so that

$$\frac{\partial}{\partial t} = \frac{\partial \eta}{\partial t}\frac{\partial}{\partial \eta} = (v_b + c)\frac{\partial}{\partial \eta}, \qquad \frac{\partial}{\partial z} = \frac{\partial \eta}{\partial z}\frac{\partial}{\partial \eta} = \frac{\partial}{\partial \eta}. \tag{10}$$

In this coordinate frame, system (7) becomes a set of ordinary differential equations

$$c\frac{\mathrm{d}m_b}{\mathrm{d}\eta} - D_b\frac{\mathrm{d}^2 m_b}{\mathrm{d}\eta^2} = -k_b m_b + k_w(1 + k_{bw}m_b^2)m_w, \tag{11a}$$

$$(c + v_w)\frac{\mathrm{d}m_w}{\mathrm{d}\eta} = k_b m_b - k_w(1 + k_{bw}m_b^2)m_w. \tag{11b}$$

We start the analysis by combining Eqs. (11) and integrating on an infinitely large domain and obtain a spatial relation between the two fields

$$m_w = -\frac{c}{c + v_w}m_b + \frac{D_b}{c + v_w}\frac{\mathrm{d}m_b}{\mathrm{d}\eta} + \frac{A}{c + v_w}. \tag{12}$$

Here A is the integration constant that is determined by the values of the concentrations far from the exponentially decaying pulse tails $[m_b(\eta \to \pm\infty), m_w(\eta \to \pm\infty)] = [m_{b,\infty}, m_{w,\infty}]$, namely $\mathrm{d}m_b/\mathrm{d}\eta \to 0$ and thus $A = (c + v_w)m_{w,\infty} + cm_{b,\infty}$. In this notation $[m_{b,\infty}, m_{w,\infty}]$ are the background uniform states on top of which the pulse is propagating. By using relation (8) we then obtain

$$A = m_{b,\infty}\left(\frac{k_b(c + v_w)}{k_w(1 + k_{bw}m_{b,\infty}^2)} + c\right), \tag{13}$$

and by combining (12) and (11a) to get an equation for m_b only

$$\begin{aligned}\left(c - \frac{k_w D_b}{c + v_w}\right)m_b' - D_b m_b'' &= \left(-\frac{k_w c}{c + v_w} - k_b\right)m_b + \frac{k_w k_{bw} A}{c + v_w}m_b^2 - \frac{k_w k_{bw} c}{c + v_w}m_b^3 \\ &+ \frac{k_w k_{bw} D_b}{c + v_w}m_b^2 m_b' + k_w\frac{A}{c + v_w},\end{aligned} \tag{14}$$

where primes denote derivatives with respect to η.

Next, we introduce an ansatz

$$m_b' = Em_b^2 + Bm_b + C, \tag{15}$$

that contains the following properties: For small m_b, far from the peak of the pulse, the distribution decays exponentially, while near the peak it is roughly behaving as a parabola. Substituting Eq. (15) into (14) and neglecting high order terms (the contributions from $m_b^2 m_b'$ to the terms proportional to m_b^3 and m_b^4), we extract the parameters E, B, C and the velocity c, by equating the two sides of the equation. The resulting equations are non-polynomial, e.g., involving square roots, and thus cannot be solved analytically. However by considering only the dominant terms in each equation, e.g., $v_w \gg c$ and $D_b k_w/c v_w \ll 1$, the resulting expressions read:

$$E \simeq \sqrt{\frac{c k_{bw} k_w}{2 D_b v_w}}, \tag{16}$$

$$B \simeq -\frac{k_b}{c}, \tag{17}$$

$$C \simeq \frac{A k_w}{c v_w}, \tag{18}$$

$$c \simeq \left(A^2\frac{2 D_b k_{bw} k_w}{v_w}\right)^{1/3}. \tag{19}$$

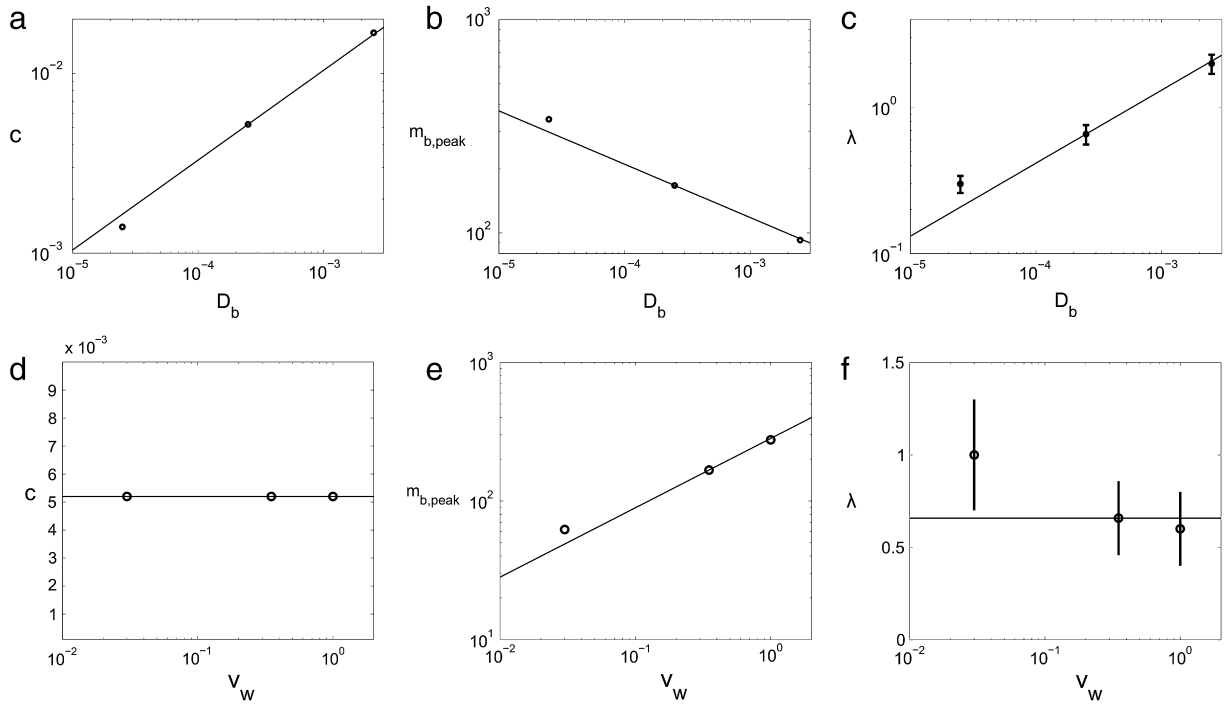

Fig. 4. Dependences of c, $m_{b,peak}$ and λ obtained from direct numerical integrations of Eq. (7) on (a–c) the stalled motors diffusion coefficient $D_b = 2.5\cdot10^{-3}, 2.5\cdot10^{-4}, 2.5\cdot10^{-5}$ (μm^2/s) (marked circles) and on (d–e) the processive motors velocity $v_w = 0.03, 0.35, 1$ (μm/s) (marked circles). The straight lines are the respective power-law dependences corresponding to Eqs. (23), (25) and (26), namely (a) 1/2, (b) $-1/4$, (c) 1/2, (d) 0, (e) 1/2, (f) 0. Other parameters as in Fig. 2.

We proceed by evaluating the last unknown $m_{b,\infty}$. We note that since on periodic domains the system conserves mass, any changes in the pulse profile modify (decrease) the initial uniform state. $m_{b,\infty}$ is obtained by substituting first the expressions for c into the expression for A and expanding in powers of $m_{b,\infty}$:

$$A \simeq \frac{k_b v_w m_{b,\infty}}{k_w} + \left(\frac{2D_b k_{bw} {k_b}^2 v_w m_{b,\infty}^5}{{k_w}^4}\right)^{1/3} (k_b - k_w)\,, \tag{20}$$

where c in terms of $m_{b,\infty}$ is given by

$$c \simeq \left(\frac{2D_b k_{bw} {k_b}^2 v_w m_{b,\infty}^2}{k_w}\right)^{1/3}. \tag{21}$$

Finally, by substituting (21) and (20) into Eq. (15) we solve for $m_b' \to 0$ (far from the pulse) to obtain

$$m_{b,\infty} \simeq \left(\frac{2D_b}{k_b}\right)^{1/4} \sqrt{\frac{k_w}{k_{bw} v_w}}. \tag{22}$$

3.2.1. Pulse speed

By inserting (22) in (21), we find that to the lowest order, the myosin treadmilling velocity c is independent of the motor velocity v_w, and obeys

$$c \propto \sqrt{k_b D_b}, \tag{23}$$

where proportionality refers solely to numerical constant and not to model parameters. After evaluating the speed, we can obtain the pulse solution:

$$m_b(\eta) = 4CB \frac{\tanh^2(q\eta/2)}{q^2 - B^2\tanh^2(q\eta/2)}, \tag{24}$$

where $q = |\sqrt{4EC - B^2}|$ effectively determines the width of the pulse (Fig. 2(c)), $\lambda = q^{-1}$; here we used the trigonometric identity $\arctan\alpha \pm \arctan\beta = (\alpha \pm \beta)/(1 \mp \alpha\beta)$.

3.2.2. Pulse width and amplitude

Under approximations used in (16)–(22), the pulse width follows

$$\lambda \simeq \frac{1}{|B|} \propto \frac{c}{k_b} \propto \sqrt{\frac{D_b}{k_b}}. \tag{25}$$

Intuitively, this result can be interpreted as following: a walking motor that hits the pulse and stalls, gets reactivated after a typical time $1/k_b$. If at that time it also re-emerges from the other side of the pulse, then the pulse width is simply given by: $\lambda \propto c/k_b$.

The pulse (24) is embedded on an unspecified background, yet, the relative pulse amplitude (the peak) which is our prime interest obeys:

$$m_{b,peak} = 4CB\frac{1}{q^2 - B^2} \simeq \frac{k_b v_w}{A k_w k_{bw}} \propto \left(\frac{k_b}{D_b}\right)^{1/4} \sqrt{\frac{v_w}{k_w k_{bw}}}. \tag{26}$$

3.3. Numerical validation

We next confront Eqs. (23), (25), (26) with direct numerical integration of Eq. (7). First, we note that pulse properties are sensitive to the initial perturbation form (inset of Fig. 3(a)). Variation of the amplitude of the initial perturbation shows that both the treadmilling velocity c and the pulse amplitude $m_{b,peak}$ reach saturation (Fig. 3(a), (b)) along the slow manifold, see Fig. 2(c). Therefore, the pulse width (λ) necessarily becomes broader due to conservation of mass (Fig. 3(c)). To allow systematic comparison, we used for λ, $m_{b,peak}$ and c, the values at which the pulse first saturated (Fig. 3(c)). Consequently, the value of the pulse width λ has the largest error and is most difficult to define uniquely (see Figs. 4, 5). Nevertheless, from biological point of view, protrusions are not closed objects and moreover, only relatively narrow pulses are being observed which are thus, within our range of validity.

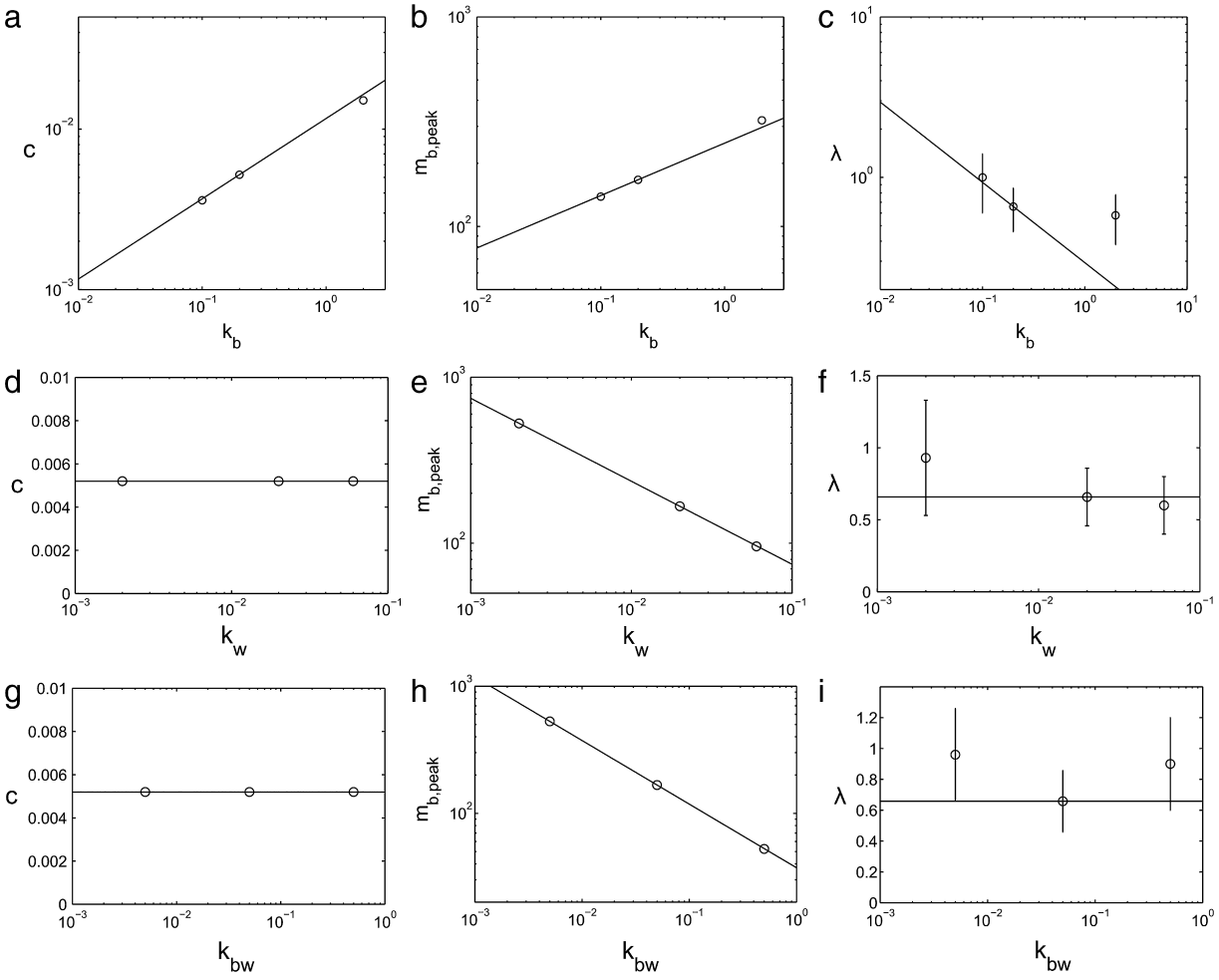

Fig. 5. Dependence of simulated (Eq. (7)) pulse characteristics, c, $m_{b,peak}$ and λ, on the different kinetic rates: (a–c) k_b, (d–f) k_w and (g–i) k_{bw} (circles). The straight lines give the predicted power-law dependences of Eqs. (23), (25) and (26), namely (a) 1/2, (b) 1/4, (c) $-1/2$, (d) 0, (e) $-1/2$, (f) 0, (g) 0, (h) $-1/2$, (i) 0. All the parameters which are not varied are as in Fig. 2.

First, we examine the dependences of the pulse properties on the diffusion coefficient D_b (Eqs. (23), (25), (26)) which agrees with direct numerical simulations, as shown in Fig. 4(a)–(c). Next, we successfully confirm an agreement with the predicted dependence on the processive motors velocity v_w, as shown in Fig. 4(d)-(f). To generalize, we also compared in Fig. 5, the dependences of c, $m_{b,peak}$ and λ on the full expressions in Eqs. (23), (25), (26), with direct numerical integrations of (7). The results are found in general to agree well, although we have not explored the whole possible parameter space. When the freely diffusing motors, m_f in Eqs. (1) is small as compared to the processive and stalled motors, the results hold also for the 3-species (full) model (e.g., pulses in Fig. 2(b)). Consequently, the derived approximate properties of the pulses provide a simplified but yet sufficient guiding description for the dependences of the pulse shape (amplitude and width) and their treadmilling velocity on the kinematic parameters of the model equations.

4. Conclusions

Chemical transport and exchange performed by molecular motors in actin-based cellular protrusions is paramount to many of the cell functionalities. We have attempted to advance the understanding of spatially localized self-organized myosin aggregates which are often observed in filopodia and stereocilia [6–11]. The results have been obtained using asymptotic analysis of a reaction–diffusion–advection model on large periodic domains. Although the model is rather simplified it provides qualitative trends for properties of isolated propagating pulses (molecular motors aggregates) which can be both supported by experiments and utilized for future empirical investigations:

- The amplitude of the pulses increases with the processive motors velocity, $\propto\sqrt{v_w}$ (see Eq. (26)). This qualitative result agrees with observations that indicate strong pulses for the highly processive myosin-X and myosin-XV that are as bright as the tip accumulation [8,10,22], as compared to weak pulses for the less processive (slower) myosin-Va [8] and myosin-III [11].
- In our model the pulses propagate with the treadmilling flow of the actin filaments in addition to an internal treadmilling of the motors, cf. [15]: new processive motors hit the pulse and are converted to stalled motors, and are thereby added to the pulse from one side. At the same time stalled motors on the other side of the pulse become processive again and leave the aggregate. As a result, the pulse is propagating faster than the actin treadmilling flow, i.e. $c > 0$ (Eq. (23)). This prediction may be tested by high resolution experiments which allow simultaneous measurements of the actin treadmilling flow and the pulse propagation.
- The width of the pulses is suggested to increase with the ability of stalled motors to perform diffusion on the actin bundle (see Eq. (25)). This prediction may be tested in future experiments by manipulating the processive motion of the motors, either through mutations or by attachment to different cargos [23].

Furthermore, while the motivation for this study was driven by a particular biological system, the results are centered on global bifurcations (homoclinic orbits) which can be utilized in a wide variety of systems that incorporate counter propagating currents, diffusion, non-linear conversion rates and mass conservation.

Acknowledgments

This work was supported in part by the Adelis foundation (A.Y.) and ISF grant 580/12 together with the historic generosity of the Perlman family (N.S.G.). N.S.G is the incumbent of the Lee and William Abramowitz Professorial Chair of Biophysics.

References

[1] R.D. Vale, The molecular motor toolbox for intracellular transport, Cell 112 (4) (2003) 467–480.
[2] P.K. Mattila, P. Lappalainen, Filopodia: molecular architecture and cellular functions, Nat. Rev. Mol. Cell Biol. 9 (6) (2008) 446–454.
[3] A.K. Rzadzinska, M.E. Schneider, C. Davies, G.P. Riordan, B. Kachar, An actin molecular treadmill and myosins maintain stereocilia functional architecture and self-renewal, J. Cell Biol. 164 (6) (2004) 887–897.
[4] R.E.M. Nambiar, Rajalakshmi, M.J. Tyska, Myosin motor function: the ins and outs of actin-based membrane protrusions, Cell. Mol. Life Sci. 67 (8) (2010) 1239–1254.
[5] M. Inaba, H. Yamanaka, S. Kondo, Pigment pattern formation by contact-dependent depolarization, Science 335 (2012) 677.
[6] J.S. Berg, R.E. Cheney, Myosin-X is an unconventional myosin that undergoes intrafilopodial motility, Nat. Cell Biol. 4 (3) (2002) 246–250.
[7] Myosin-X: a molecular motor at the cell's fingertips, Trends Cell Biol. 15 (10) (2005) 533–539.
[8] A novel form of motility in filopodia revealed by imaging Myosin-X at the single-molecule level, Curr. Biol. 19 (11) (2009) 967–973.
[9] T.M. Watanabe, H. Tokuo, K. Gonda, H. Higuchi, M. Ikebe, Myosin-X induces filopodia by multiple elongation mechanism, J. Biol. Chem. 285 (25) (2010) 19605–19614.
[10] I.A. Belyantseva, E.T. Boger, S. Naz, G.I. Frolenkov, J.R. Sellers, Z.M. Ahmed, A.J. Griffith, T.B. Friedman, Myosin-Xva is required for tip localization of whirlin and differential elongation of hair-cell stereocilia, Nat. Cell Biol. 7 (2) (2005) 148–156.
[11] F. Salles, R. Merritt, U. Manor, G. Dougherty, A. Sousa, J. Moore, C. Yengo, A. Dosé, B. Kachar, Myosin IIIa boosts elongation of stereocilia by transporting espin 1 to the plus ends of actin filaments, Nat. Cell Biol. 11 (4) (2009) 443–450.
[12] A. Yochelis, S. Ebrahim, B. Millis, R. Cui, B. Kachar, M. Naoz, N.S. Gov, Self-organization of waves and pulse trains by molecular motors in cellular protrusions, Sci. Rep. 5 (2015) 13521.
[13] K. Zeldovich, J.-F. Joanny, J. Prost, Motor proteins transporting cargos, Eur. Phys. J. E 17 (2) (2005) 155–163.
[14] I. Pinkoviezky, N. Gov, Transport dynamics of molecular motors that switch between an active and inactive state, Phys. Rev. E 88 (2013) 022714.
[15] I. Pinkoviezky, N.S. Gov, Traffic jams and shocks of molecular motors inside cellular protrusions, Phys. Rev. E 89 (2014) 052703.
[16] K. Doubrovinski, K. Kruse, Cytoskeletal waves in the absence of molecular motors, Europhys. Lett. 83 (1) (2008) 18003.
[17] A. Yochelis, M. Sheintuch, Towards nonlinear selection of reaction–diffusion patterns in presence of advection: A spatial dynamics approach, Phys. Chem. Chem. Phys. 11 (2009) 9210.
[18] A. Yochelis, M. Sheintuch, Principal bifurcations and symmetries in the emergence of reaction–diffusion–advection patterns on finite domains, Phys. Rev. E 80 (2009) 056201.
[19] P.K. Maini, K.J. Paintera, H.N.P. Chau, Spatial pattern formation in chemical and biological systems, J. Chem. Soc. Faraday Trans. 93 (1997) 3601–3610.
[20] C.K.R.T. Jones, N. Kopell, R. Langer, Construction of the FitzHugh–Nagumo pulse using differential forms, in: Patterns and Dynamics in Reactive Media, Springer, New York, 1991.
[21] P. Carter, B. Sandstede, Fast pulses with oscillatory tails in the Fitzhugh–Nagumo system, SIAM J. Math. Anal. 47 (2015) 3285–3441.
[22] M. Kerber, D. Jacobs, L. Campagnola, B. Dunn, T. Yin, A. Sousa, O. Quintero, R. Cheney, A novel form of motility in filopodia revealed by imaging Myosin-X at the single-molecule level, Curr. Biol. 19 (11) (2009) 967–973.
[23] M. Sckolnick, E.B. Krementsova, D.M. Warshaw, K.M. Trybus, More than just a cargo adapter, melanophilin prolongs and slows processive runs of Myosin va, J. Biol. Chem. 288 (41) (2013) 29313–29322.